PSF and non-uniformity in a monolithic, fully depleted, 4T CMOS image sensor

Conference or Workshop Item

PSF and Non-Uniformity in a Monolithic, Fully Depleted, 4T CMOS Image Sensor

J. Ivory*[a], K. D. Stefanov[a], P. Turner[b], A.D. Holland[a]
[a]Centre for Electronic Imaging, The Open University, Walton Hall, Milton Keynes, MK7 6AA, UK;
[b]Teledyne e2v 106 Waterhouse Ln, Chelmsford CM1 2QU, UK

ABSTRACT

Lateral charge diffusion is one of the main contributors to the Point Spread Function (PSF) in CMOS image sensors, due to the small depth to which they can be depleted. This can have an adverse effect on the spatial resolution of the sensor and the measured shape of the observed object. In this paper, PSF measurements are made on a novel CMOS detector capable of reverse bias and full depletion. The PSF is measured with the Virtual Knife Edge (VKE) technique at five wavelengths, from 470 nm to 940 nm, to ascertain wavelength dependence. The inter- and intra-pixel non-uniformity is examined to determine the difference between pixels as well as within the pixels themselves. Finally, the pixel structure is also evaluated using a 1 µm spot of light to examine the effect of the internal layout of a pixel on the sensitivity to light. These factors all impact precision astronomical measurements and so need to be understood before use in science missions.

Keywords: Point Spread Function, Photo Response Non-Uniformity, Charge Diffusion, CMOS, VKE

1. INTRODUCTION

Charge Coupled Devices (CCDs) have long been the technology of choice for precision astronomical measurements. However, with recent advancements in CMOS Image Sensors (CIS), many ground and space based telescopes are beginning to investigate them as a possible replacement for CCDs in certain applications, such as GravityCam [1], TAOS II [2] and Juice [3]. With inherent advantages over CCDs, such as better radiation hardness, lower power consumption and selective readout [4], they can be used in a wide range of applications. There are however a few parameters in which CMOS sensors are yet to perform as well as CCDs. These include Quantum Efficiency (QE) (particularly at long wavelengths) [5, 6], the Point Spread Function (PSF) and non-uniformity, both inter- and intra-pixel [7].

1.1 PSF

In an ideal sensor, the image produced would be an exact copy of the light which was incident upon it. This is not the case however, due to a number of factors relating to the sensor such as pixel size, pixel structure and electric fields within the pixel. The PSF of a sensor is a measure of how much a point source of light is spread and distorted by a sensor when it is measured. The main contribution to PSF in most image sensors is lateral diffusion, whereby photo-generated electrons are able to move within the silicon lattice and be captured some distance away from the generation site. If this spread is isotropic, the measured image will be larger than it should. If it is not, the shape of the image will change. The extent to which an image is changed must be quantified in order to recreate the original image from the one that is measured, and is particularly important to precision astronomy.

In most modern CCDs, the pixel is homogeneous with a depletion region that extends through the entire thickness of the silicon. This serves to limit the lateral diffusion, particularly in Back Side Illuminated (BSI) CCDs. In traditional monolithic CMOS sensors, where reverse bias and full depletion are not possible, there are large field-free regions in which lateral diffusion can occur. The field-free regions can be minimised to an extent by keeping the CMOS sensor thickness low compared to CCDs [8], but at the cost of sacrificing some QE. The CMOS pixel is also far more complex than that of a CCD, containing a number of transistors, which can detrimentally affect the PSF.

1.2 Photo Response Non-Uniformity

Silicon detectors are made up of an array of pixels, each of which should be identical to every other one. However due to manufacturing imperfections there can be slight variations from one pixel to the next, affecting the sensitivity to light. This is known as inter-pixel non-uniformity. In CCDs, this effect is mostly due to differences in thickness of the silicon and the gates leading to larger or smaller electric fields. The effect, known as Fixed Pattern Noise (FPN) is usually small in CCDs, but not insignificant. With a CMOS pixel, contributors to FPN include the size of the Pinned Photodiode (PPD) as well as the metal tracks. The differences between pixels is important to characterise so they can be accounted for in image processing.

Within the pixels themselves, there may also be some variation in signal measured depending on where the photons interact. With its simpler pixels, a CCD will experience very little intra-pixel non-uniformity as most photons will interact with a depleted region of silicon, but it is not a negligible effect [9]. Photons incident upon CMOS pixels, with their more complex internal structure, have a chance of interacting with silicon that is part of the readout circuitry [10]. This leads to these photons not being measured during readout, lowering the resulting flux value. This can impact precision astronomy as it means that objects may be measured as brighter or dimmer depending on their location within the pixel.

1.3 Fully Depleted CMOS Sensor

The sensor tested is a BSI CMOS sensor developed at The Open University [11]. It is comprised of eight sections, each with 16x32, 4T pixels, four with 10 µm pixels and four with 5.4 µm pixels. Only the 10 µm pixel results are presented here. The device can be reverse biased, in these tests at a constant -6 V, the first 4T CMOS sensor on which this has been achieved. The reverse bias allows the full thickness, 12 µm in this test chip, of the silicon to be depleted, increasing the QE while maintaining a good PSF. This device was chosen as its novel architecture should achieve similar characteristics to that of a fully depleted CCD of the same thickness, allowing for closer comparisons of the two technologies in the future.

2. METHODOLOGY

2.1 Test Setup

The setup for these tests was essentially a microscope in reverse and is presented in Figure 1. At one end there is an interchangeable LED threaded into the end of the optical tube. The threading ensures the LED is parallel to the tube when mounted. A total of five different LEDs were used in these tests, with wavelengths ranging from 470 nm to 940 nm. The photons pass through a ground glass diffuser in order to flat-field the light. The light then passes through a pinhole, down to an infinity-corrected tube lens. This lens collimates the light, which is then focused down by a de-magnification factor of 5. The spot of either 1, 5 or 10 µm diameter is then projected onto the sensor.

The sensor itself is mounted on an XYZ translation stage, with 25 mm travel range in all axes and a resolution of 70 nm. In these tests, X and Y are parallel to the plane of the sensor face, while Z is perpendicular which allows focusing of the spot. All movement is controlled via LabVIEW based DAQ system, which also controls the power and the control circuitry of the sensor. The orthogonality of the sensor to the light is measured as >99.997 %, so no corrections were implemented.

Before each measurement, the spot is focused onto the sensor. This is done by first moving the sensor in the Z plane until the spot is roughly in focus. The sensor is then moved by -40 µm in the Z direction, and moved in 1 µm steps to +40 µm, with a reading at each point. A graph of intensity vs Z position is plotted and the maxima used as the position of best focus.

The setup is housed within a dark box, which blocks all external light and so only photons from the spot are detected. All tests are run at room temperature, as cooling is not necessary due to low dark current and the high frame rate.

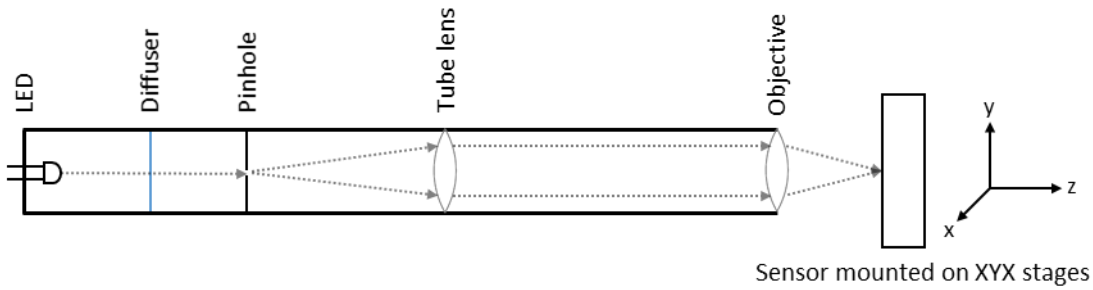

Figure 1 – Schematic diagram of test setup.

2.2 Virtual Knife Edge

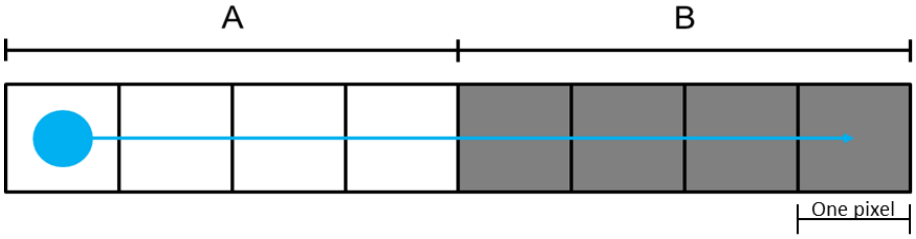

Figure 2 – The Virtual Knife Edge (VKE) technique. All of the signal in Section A is summed and plotted against the displacement of the spot for each point.

For measuring the PSF of a sensor, the Virtual Knife Edge (VKE) technique [12] is used. With this method, a small spot of light is projected on to the sensor and scanned across a portion of a single row or column, as in Figure 2. The spot is scanned from one end to the other, across both sections A and B. The signal in all pixels in Section A is then summed together, ignoring all signal in Section B, as if a knife edge was placed at the boundary, covering all pixels in Section B. The total signal is then plotted against the distance the spot has travelled, as in Figure 3a. The differential of this graph is then plotted against spot displacement, and a Gaussian fit applied to find the standard deviation – as in Figure 3b. The full width half maximum (FWHM) is calculated from this and taken as the PSF.

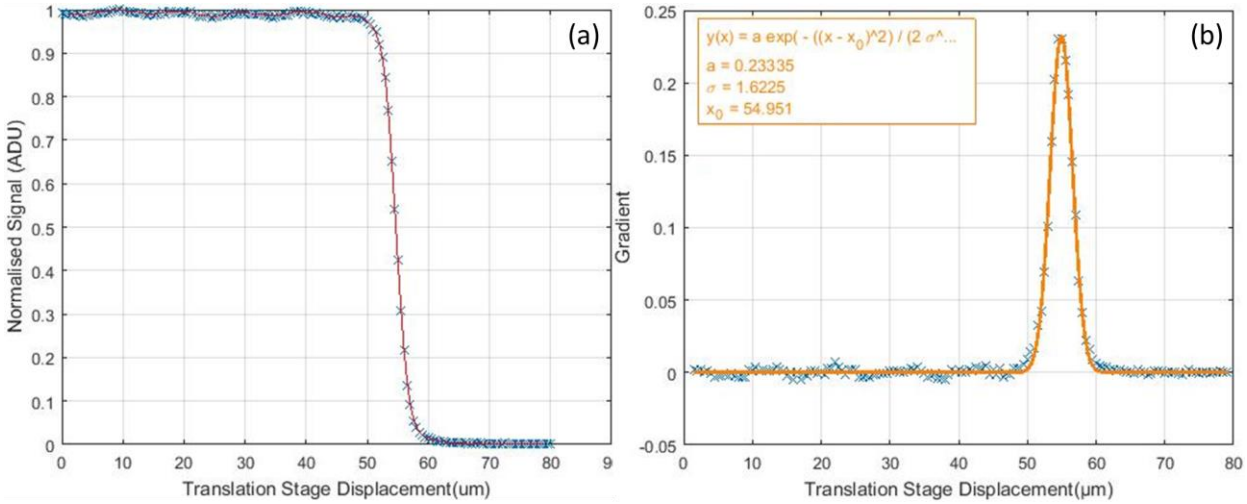

Figure 3 – (a) The signal in Section A of the VKE measurement vs the spot displacement. The signal has been normalized to allow easy comparisons, (b) the differential of the graph on the left. From this, the standard deviation can be found and thus the FWHM.

2.3 Line and Raster Scanning

To examine inter- and intra-pixel non-uniformity, a single line of pixels can be scanned, similar to the VKE technique. However, in this test, all pixels are measured and the intensity plotted against the displacement of the spot. This gives a one dimensional cut of the sensor and the sensitivity of each point along that line. From this, the peak value for each pixel can be seen allowing inter-pixel non-uniformity to be seen. It also shows the intra-pixel non-uniformity as the shape of the peak within a single pixel.

To image the internal structure of the pixels, a 2-D map of the sensitivity is generated. For this, a 1 µm spot is scanned across a number of pixels in a raster fashion and the signal at each point measured. The signal and displacement values are then plotted, showing the sensitivity to light of that section of the pixel. The step size between each scan line is 250 nm. This allows for a fine resolution when recreating the sensitivity of each point within a pixel.

3. RESULTS AND DISCUSSION

3.1 PSF

The lateral charge diffusion was measured over a number of different spot sizes at five different wavelengths. Each data point consists of scans in three separate columns, averaged and the standard deviation used as statistical error bars. Scans were performed in the Y direction only. Results are shown in Figure 4.

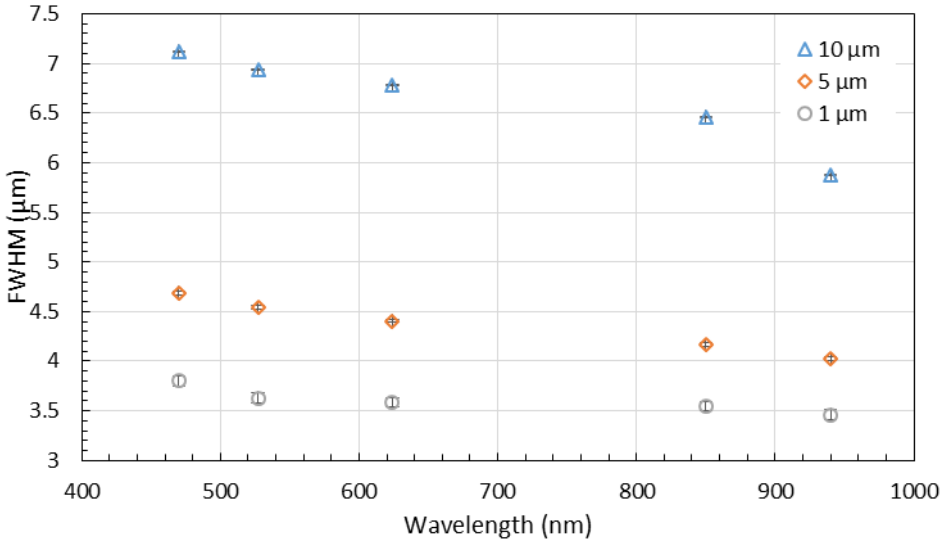

Figure 4 – Comparison of PSF measured at multiple wavelengths with varying spot size. PSF decreases as wavelength is increased, which needs further investigation. Statistical error bars are present, calculated as the standard deviation of the FWHM taken from three columns.

The results show that PSF gets smaller the longer the wavelength used. This is what would be expected in an undepleted device. This fully depleted device should not exhibit this behaviour as strongly and so further tests and simulations are needed to determine the reason for this.

With tests done at three spot sizes, the dependence on spot size of the PSF can be examined. Plotting the size of the spot vs the PSF at each wavelength, as in Figure 5, a trend can be seen. It is hoped that, with further tests at a greater number of spot sizes, an equation can be found to explain the trend of the graph. With an equation, a PSF can be found for an infinitesimally small spot, which can be said to be the true sensor PSF.

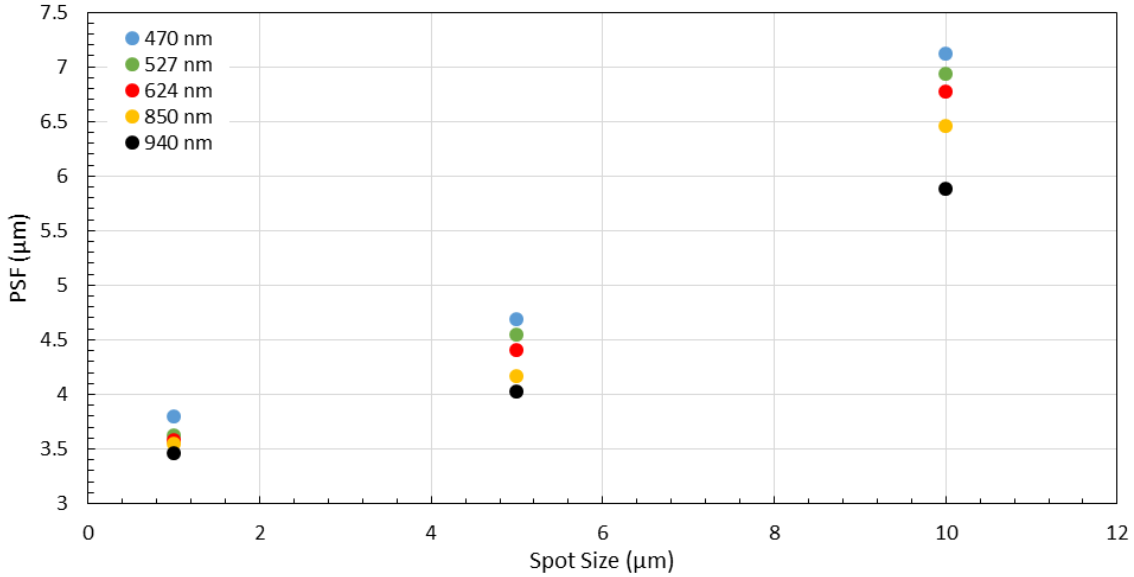

Figure 5 – Comparisons of the PSF at different spot sizes for all wavelengths. There appears to be a trend in the data for which an equation could be found allowing calculation of PSF at any spot size, which would be useful for astronomical imaging of objects of varying sizes.

3.2 Line Scanning

Using the line scanning technique, the difference between pixels as well as within pixels is examined. By looking at the difference between the maxima of each peak, the inter-pixel non-uniformity can be discerned. Looking at the differences in signal on the scale less than pixel size, intra-pixel non-uniformity can be seen.

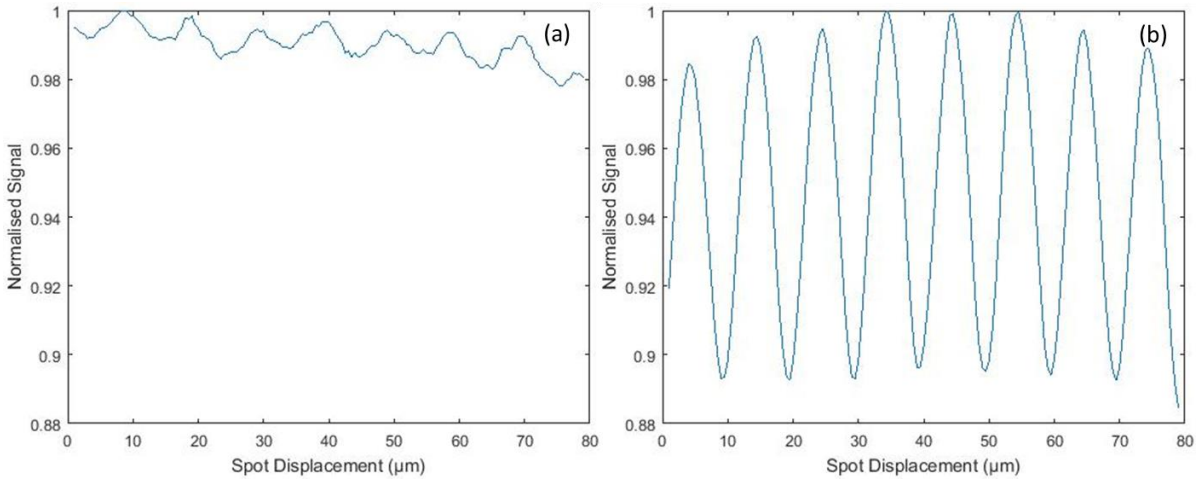

Figure 6 – Line scans at two different wavelengths. Plot (a) shows a scan with 470 nm light. Variations at the sub-pixel level are evident. Plot (b) shows a scan taken at 940 nm, where the signal exhibits far more dependence on position within the pixel.

Figure 6 shows a comparison between line scans at 470 nm and 940 nm. The scans begin in the centre of the first pixel. At 470 nm, the signal is not smooth, showing a large amount of sub-pixel variation and pixel scale variation. Peak to trough variations are measured at 2%. Peaks also occur in the centre of the pixel, where the photodiode is located. Tests with 940 nm light give much smoother results, with very little intra-pixel features. Peak to trough variations are higher than 470 nm, at 11%. One interesting feature is that signal peaks at the boundary between two pixels, rather than in the photodiode. The reasons for this are explained in the next section when a pixel sensitivity map is created. Results for 527 nm and 624 nm are similar to those of the 470 nm light, and results for 850 nm are similar to those of 940 nm but to a smaller extent. This is shown in Figure 7.

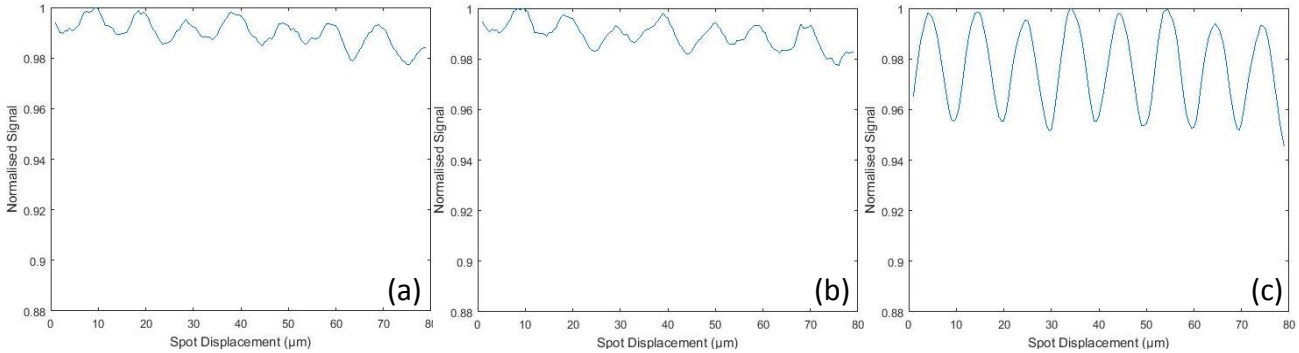

Figure 7 – Line scans performed at (a) 527 nm (b) 624 nm and (c) 850 nm. The two shorter wavelengths give similar results to the 470 nm scan, and the 850 nm scan is similar to that of the 940 nm scan.

3.3 Pixel Mapping

To map individual pixels the raster scanning technique is used. One would expect the sensitivity of the pixel to remain mostly uniform over the entire area, particularly at shorter wavelengths as most photons will be absorbed in the depletion region, and not reach the transistors within the pixel. Both 470 nm and 624 nm light are absorbed within 12 µm, the thickness of this device. This is the case, as is shown in Figure 8. Pixel boundaries are not obvious in the two scans, and the variation in the signal is <5% at 470 nm and <7% at 624 nm. This variation is larger than the values seen in the line scans, and can be attributed to when the spot is in the corner of the pixel, where the line scans are through the centre of the pixels. If a cross section of a pixel map is taken at the centre of a pixel and plotted as a line scan, a variation of 2% is measured, shown in Figure 9.

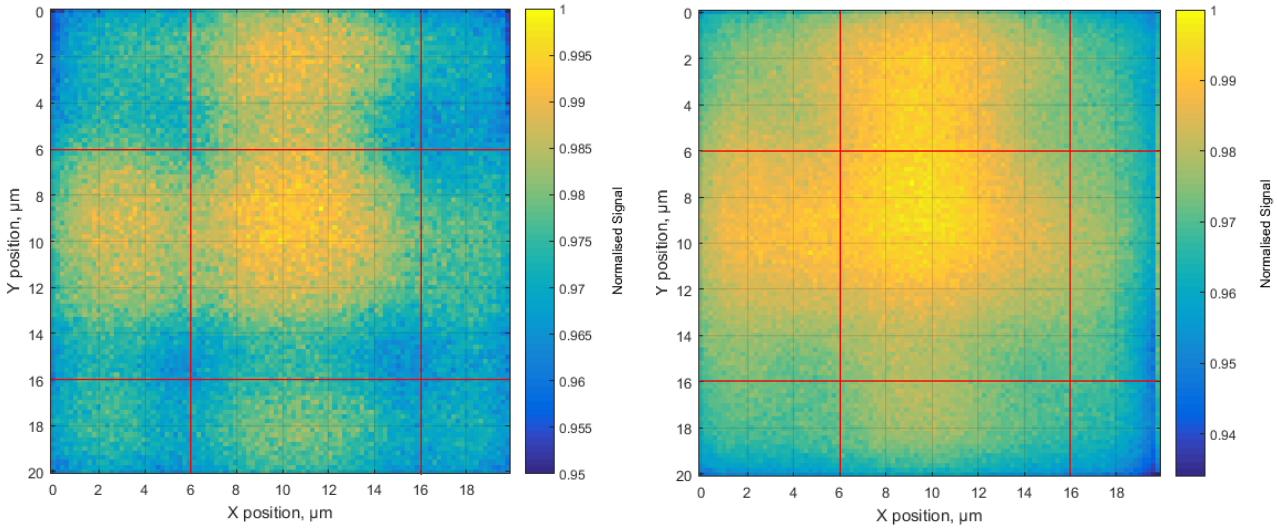

Figure 8 – Two raster scans of a central pixel, one at 470 nm (left) and one at 624 nm (right). The red lines indicate the physical pixel boundaries. Both images are quite flat, exhibiting less than 7% difference.

As the wavelength of light used is increased, pixel features become visible in the scans. Figure 11 shows a scan at 940 nm. Figure 10 demonstrates that the absorption depth of 940 nm light in silicon is 5-6 times higher [13] than the thickness of the device, meaning a large proportion of the light will travel through the entire thickness, some of which will interact with the metal tracks within the pixel.

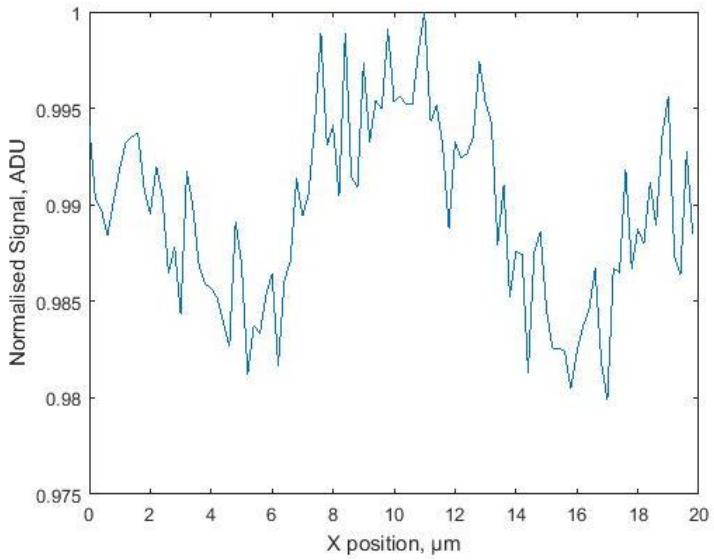

Figure 9 – A line scan taken from a cross section of a raster scan at 470 nm. This demonstrates that although peak to trough variation is higher in the pixel map, through the centre of the pixel it matches the values found in the line scan.

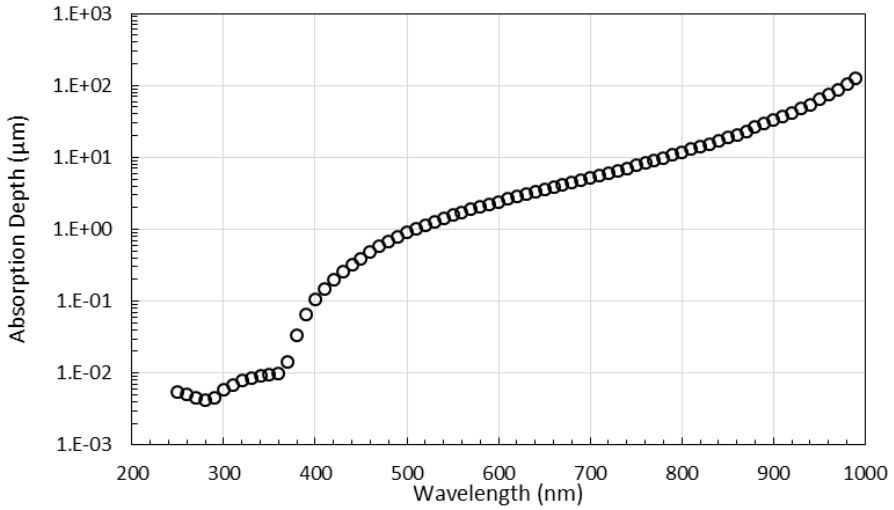

Figure 10 – Absorption depth for photons in silicon. Any light below 800 nm has an absorption depth below the thickness of the sensor, whereas for 940 nm photons, it is far greater. Data for this graph taken from [13].

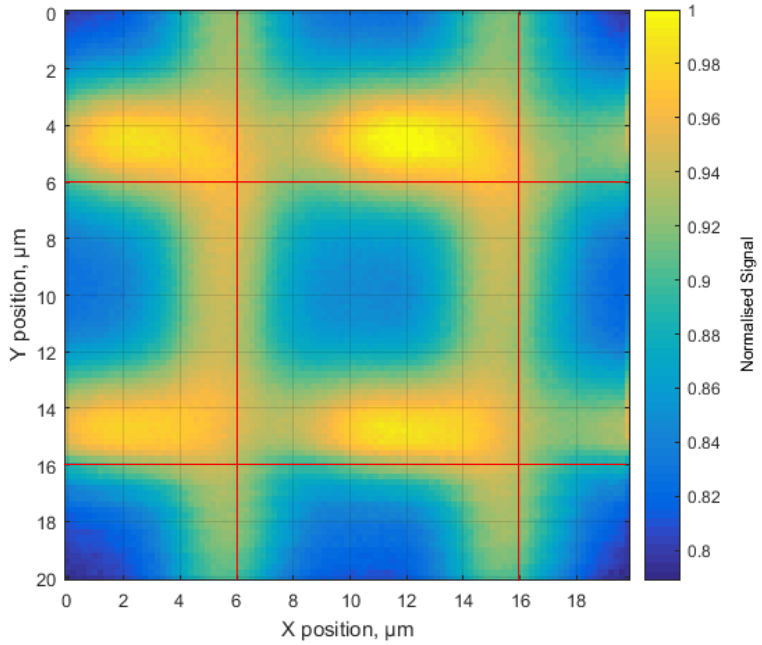

Figure 11 – Raster scan taken with 940nm light. In this case, the pixel boundaries are visible from the scan, with variations of up to 20% between the PPD and the edges of the pixel.

The signal variation in this image is far higher at ~20%. The reason for this is believed to be the metal tracks on the front side of the sensor. As the light comes in the back side, it is measured once by the silicon. The photons that have not interacted continue out the other side. The light that passes through areas that have metal track on the front side is reflected and enters the sensor once again. This reflected light has another chance to interact with the silicon, effectively measuring the light twice. This is shown when the layout of the metal tracks of the pixel are superimposed over the signal map as in Figure 12.

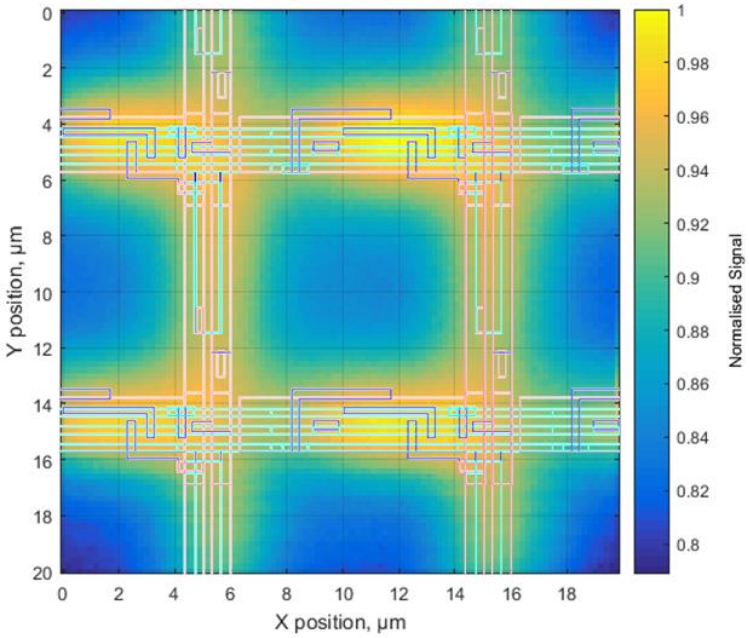

Figure 12 – Raster scan at 940 nm with the pixel's metal track structure overlaid. The overlay shows that the bright points in the scan correlate to the layout of the metal of the pixel.

4. CONCLUSIONS

The work presented in this paper has shown a number of inter- and intra-pixel effects in a CMOS sensor found through spot scanning. PSF measurements indicate that even for small spot sizes, fully depleted CMOS sensors exhibit non-negligible charge diffusion that must be accounted for if used for precision astronomy measurements, similar to CCDs [14]. Using a number of different spot sizes with the VKE method seems to show a trend which needs to be investigated further and could lead to a fit, yielding the true sensor PSF at an infinitesimally small point of light, as well as the spread of any size light spot.

Line scans indicate different inter-pixel uniformity for different wavelengths of light. Shorter wavelengths exhibit a smaller difference between pixel peaks than longer wavelengths do. Longer wavelength tests also exhibit more sub-pixel variations than at longer wavelengths. This may be due to charge diffusion into columns adjacent to the ones being tested, or from reflections from metal tracks.

The most interesting results are those from the pixel mapping. At the shorter wavelengths, the pixel looks relatively flat and no structure can be seen. However, as the wavelength is increased to a point where the absorption depth is longer than the thickness of the device, it is possible to see the internal structure of the pixel. This is due to the reflection of light from the metal tracks on the front side of the device and could potentially have a detrimental effect on astrometry and photometry measurements. It is important therefore to ensure that for any measurements, the sensor is carefully chosen such that the longest wavelength being measured has an absorption depth shorter than the thickness of the silicon.

Overall, it is evident that CMOS sensors do exhibit a large number of inter- and intra-pixel variations that can be detrimental to any scientific measurements made on them. These effects must therefore be properly studied and characterized for any device being used in order to minimise the impact they can have on results. The next step in these studies will be to examine a CCD with similar physical characteristics to make direct comparisons between the two.

[REFERENCES]

1. MacKay, C., M. Dominik, and I. Steele. *GravityCam: wide-field, high-resolution imaging and high-speed photometry instrument*. in *SPIE Astronomical Telescopes + Instrumentation*. 2016. SPIE.
2. Hall, H.J., et al. *Status of the Transneptunian Automated Occultation Survey (TAOS II)*. in *Ground-based and Airborne Telescopes VI*. 2016. SPIE.
3. Soman, M., et al. *Design and characterisation of the new CIS115 sensor for JANUS, the high resolution camera on JUICE*. in *SPIE Astronomical Telescopes + Instrumentation*. 2014. SPIE.
4. Bigas, M., et al., *Review of CMOS image sensors.* Microelectronics Journal, 2006. **37**(5): p. 433-451.
5. e2v, *CIS113 Large Area and Buttable CMOS Image Sensor.* 2016.
6. e2v, *CCD231-C6 Back-illuminated Scientific CCD Sensor.* 2014.
7. Zhan, H., X. Zhang, and L. Cao, *Intrapixel effects of CCD and CMOS detectors.* Journal of Instrumentation, 2017. **12**(04): p. C04010-C04010.
8. Jorden, P.R., et al. *e2v new CCD and CMOS technology developments for astronomical sensors*. in *SPIE Astronomical Telescopes + Instrumentation*. 2014. SPIE.
9. Jorden, P.R., J.-M. Deltorn, and A.P. Oates. *Nonuniformity of CCDs and the effects of spatial undersampling*. in *1994 Symposium on Astronomical Telescopes and Instrumentation for the 21st Century*. 1994. SPIE.
10. Shcherback, I., T. Danov, and O. Yadid-Pecht, *A Comprehensive CMOS APS Crosstalk Study: Photoresponse Model, Technology, and Design Trends.* IEEE Transactions on Electron Devices, 2004. **51**(12): p. 2033-2041.
11. Stefanov, K.D., et al., *Design and Performance of a Pinned Photodiode CMOS Image Sensor Using Reverse Substrate Bias.* Sensors (Basel), 2018. **18**(1).
12. Karcher, A., et al., *Measurement of lateral charge diffusion in thick, fully depleted, back-illuminated CCDs.* IEEE Transactions on Nuclear Science, 2004. **51**(5): p. 2231-2237.
13. A., G.M. and K.M. J., *Optical properties of intrinsic silicon at 300 K.* Progress in Photovoltaics: Research and Applications, 1995. **3**(3): p. 189-192.

14. Holland, S.E., et al., *Physics of fully depleted CCDs.* Journal of Instrumentation, 2014. **9**(03): p. C03057-C03057.